Received: 27 February 2023 | Revised: 12 July 2023 | Accepted: 3 August 2023

DOI: 10.1002/jmor.21633

RESEARCH ARTICLE

JOURNAL OF morphology WILEY

Three-dimensional visualization of predatory gastropod feeding teeth with synchrotron scanning

Gregory S. Herbert[1] | Stephen A. Hill[1] | Maria Jose Pio[2] | Ryan Carney[3] | Amber Carlson[1] | Elis Newham[4,5] | Jen A. Bright[1]

[1]School of Geosciences, University of South Florida, Tampa, Florida, USA

[2]Consejo Nacional de Investigaciones Científicas y Técnicas, CONICET, Buenos Aires, Argentina

[3]Department of Integrative Biology, University of South Florida, Tampa, Florida, USA

[4]School of Engineering and Materials Sciences, Queen Mary University of London, London, UK

[5]Section Palaeontology, Institute of Geosciences, Rheinische Friedrich-Wilhelms-Universität Bonn, Bonn, Germany

Correspondence

Gregory S. Herbert and Jen A. Bright, School of Geosciences, University of South Florida, Tampa, FL 33620, USA.
Email: gherbert@usf.edu and j.bright@hull.ac.uk

Present addresses

Stephen A. Hill, Department of Earth and Planetary Sciences, University of Tennessee, Knoxville, Tennessee, USA.

Jen A. Bright, School of Natural Sciences, University of Hull, Hull, UK.

Abstract

Several families of neogastropod mollusks independently evolved the ability to drill through mineralized prey skeletons using their own mineralized feeding teeth, sometimes with shell-softening chemical agents produced by an organ in the foot. Teeth with more durable tooth shapes should extend their use and improve predator performance, but past studies have described only the cusped-side of teeth, mostly overlooking morphologies related to functional interactions between teeth. Here, we describe the three-dimensional morphology of the central drilling tooth (rachidian) from four species of the neogastropod family Muricidae using synchrotron tomographic microscopy and assemble a three-dimensional model of a multitooth series in drilling position for two of them to investigate their dynamic form. We find two new types of articulating surfaces, including a saddle joint at either end of the rachidian and a large tongue-and-groove joint in the center. The latter has a shape that maximizes contact surface area between teeth as they rotate away from each other during drilling. Articulating joints have not been described in Neogastropod radula previously, but they are consistent with an earlier hypothesis that impact forces on individual teeth during predatory drilling are dispersed by tooth–tooth interactions.

KEYWORDS

Gastropoda, morphology, Muricidae, radula, synchrotron

1 | INTRODUCTION

Nearly all predatory families of gastropods arose in the late Cretaceous (Taylor, 1998), which was a time of rapid evolutionary innovation and ecological restructuring now known as the Mesozoic marine revolution (MMR: Vermeij, 1977). One of the feeding innovations that evolved repeatedly during the MMR was predatory drilling (Kabat, 1990; Morton & Chan, 1997; Ponder & Taylor, 1992), which refers to the ability of some gastropods to excavate feeding holes through the mineralized armor of shelled invertebrate prey. In the neogastropod family Muricidae, the most diverse clade of drillers, drilling is thought to be the plesiomorphic mode of feeding (Vermeij & Carlson, 2000) and enabled by alternating rounds of chemical dissolution by an accessory boring organ and mechanical abrasion by the radula, which consists of hundreds of rows of mineralized teeth attached to a long, flexible ribbon (Carriker, 1981; Carriker & Gruber, 1999; Carriker & Van Zandt, 1972; Figure 1). Each tooth row has a multi-cusped rachidian tooth in the center flanked by a sickle-shaped lateral tooth on either side. During the mechanical phase of drilling, the radular ribbon is pulled back and forth (Simone, 2011, p. 194) over the tip of a tongue-like cartilage (the odontophore) like the teeth of a chain saw (Huxley, 1853), with each pull causing contact of 5–15% of radula tooth rows with the prey shell surface (Fujioka, 1985; Harding et al., 2008; Hemingway, 1975). Most of the

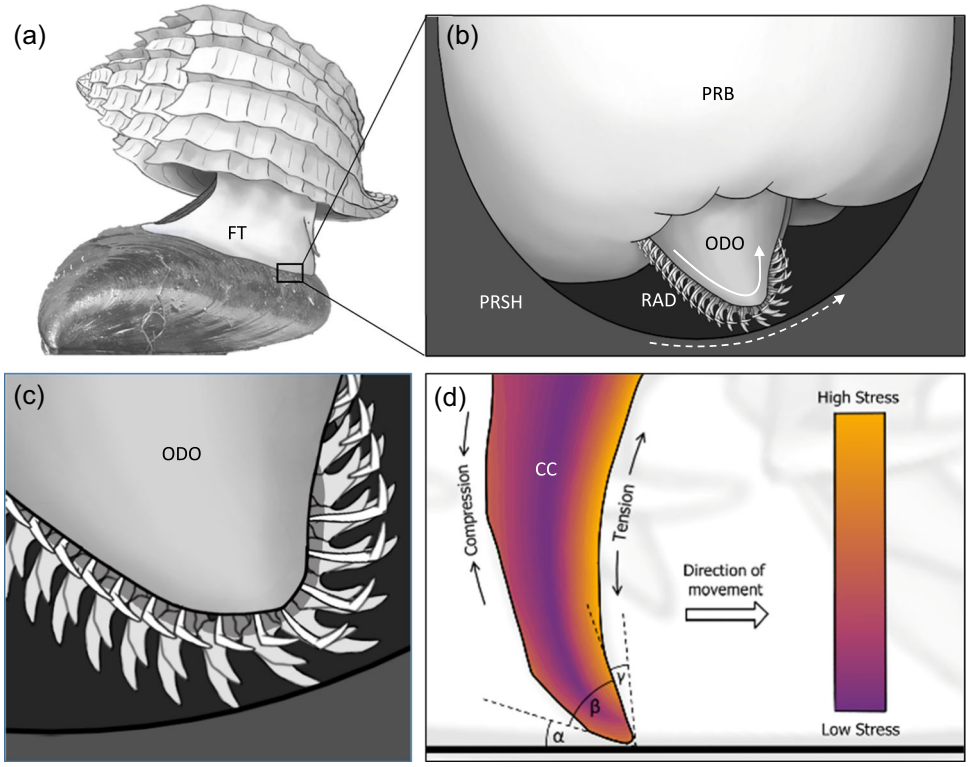

FIGURE 1 Drawing showing the anatomical position of the feeding apparatus of the Muricidae during predatory drilling of a prey bivalve mollusk (a), excavation of shell inside an active borehole with a sweeping motion of the tooth-covered, odontophore-like tongue (dotted line) and simultaneous rotation of radular teeth over the tip of the odontophore (solid line) modeled after Carriker and Van Zandt (1972: figs. 12 and 17) (b), closeup of individual central teeth (rachidia) of the radula striking the shell (c), and a schematic representation of how mechanical stresses on the rachidian tooth central cusp are likely to be accommodated as bending within striking cusps (d). CC, central cusp; FT, foot; ODO, odontophore; PRB, proboscis; PRSH, prey shell; RAD, radula; RT, rachidian tooth; α, clearance angle; β, wedge angle; ϒ, rake angle.

tooth–substrate contact is with the rachidian tooth; lateral teeth are pulled back and make only incidental contact with the surface (Carriker et al., 1974). Simultaneously, the odontophore cartilage performs its own complicated motion, performing either a cleaning sweep across the prey shell surface or striking at it as a geologist would use a rock hammer (Carriker & Schaadt, 1973; Carriker et al., 1974).

Tooth rows damaged from drilling (Figure 2; Carriker et al., 1974) are continuously replaced in a conveyor-belt fashion, with upstream production of new teeth in the radular sac and downstream shedding of older teeth into the esophagus. However, tooth damage from drilling can outpace the rate new teeth are moved into striking position (Fujioka, 1985), leaving snails to reuse damaged teeth until nothing is left but a flat base (Figure 2d–f; see also Carriker et al., 1974). Selection should, therefore, favor (1) teeth with stronger material properties (e.g., microstructural fibers, mineral reinforcement, degree of tanning; Krings, Matsumura, et al., 2022; Tyler & Schiffbauer, 2012), (2) faster tooth replacement (Fujioka, 1985), (3) evolution of feeding modes that reduce drilling times (e.g., edge drilling, toxins, prying and wedging, scavenging, parasitism; Herbert, 2004, 2009; Dietl & Herbert, 2005; Paul et al., 2015); and/or (4) teeth with more durable shapes that extend their use (e.g., self-sharpening wear, cusps with wider and stronger bases, articulating bases, etc.; Herbert et al., 2007, 2016).

Complex articulating structures at the margins and bases of adjacent radular teeth are already known from scanning electron micrographs (SEM) of muricid radulae (Herbert et al., 2015; Pio et al., 2014). Possible functions of these structures include distributing impact forces between teeth to prevent early wear (Carriker et al., 1974) and counteracting lateral bending or torsional forces along the radula by keeping teeth aligned (Hickman, 1980, 1984). Interestingly, complex tooth–tooth articulation is absent or poorly developed in neogastropods that use the radula for piercing, raking, or scooping soft flesh, reinforcing the hypothesis that the complex articulations of muricid radulae are adaptations for drilling.

This study uses synchrotron tomographic microscopy (see Donoghue et al., 2006) to develop the first three-dimensional (3D) models of muricid radulae, a first step in testing whether ~70 million years of drilling has led to more durable tooth shapes and better drillers. Synchrotron radiation produces extremely bright X-rays, allowing much higher tomographic resolutions and better contrast than conventional medical- or micro-CT scanners (Cunningham et al., 2014). Reconstructing tomographic X-ray data allows us to visualize complete quantitative surfaces of muricid radulae from any orientation for the first time, including articulation surfaces between

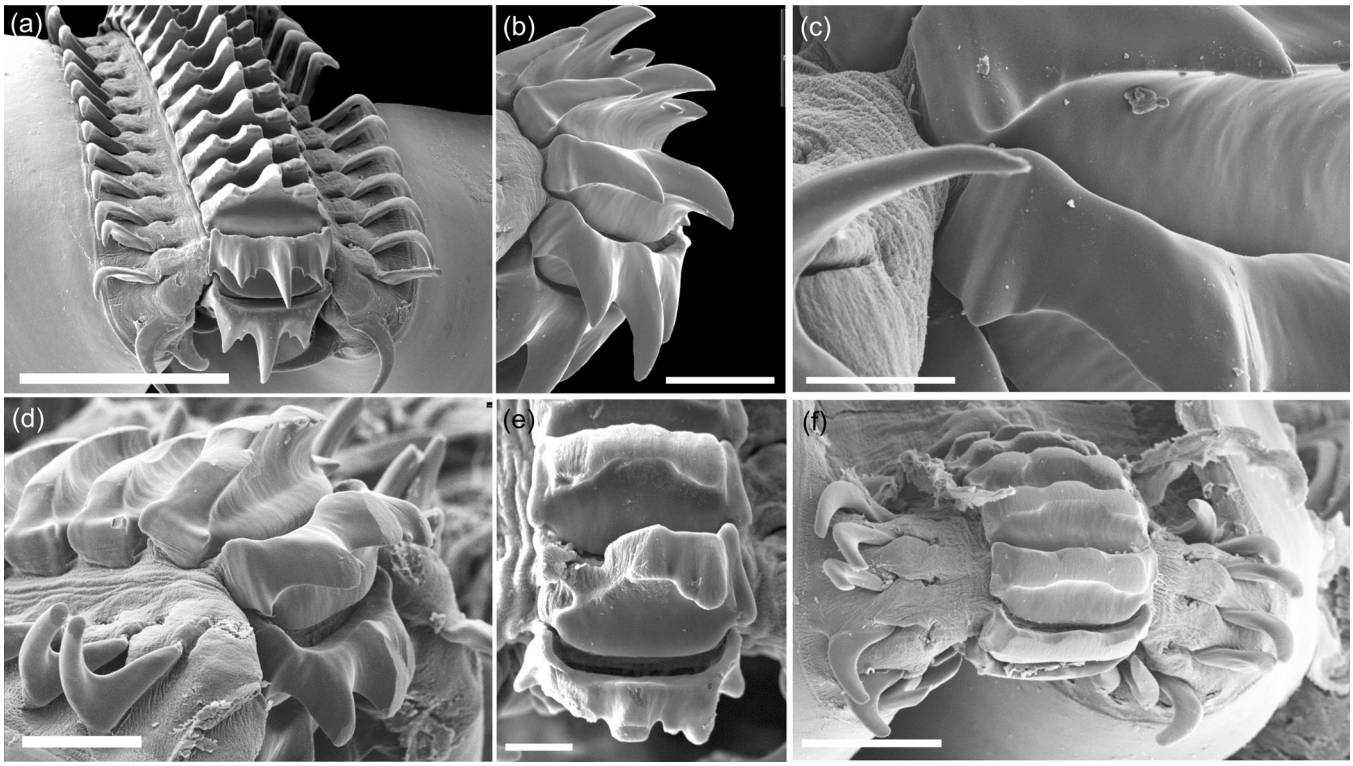

FIGURE 2 Scanning electron micrographs (SEM) showing radular tooth–tooth contact and teeth before and after predatory shell drilling in the muricid *Trophon geversianus*. View of intact tooth rows, including the central rachidian tooth and sickle-shaped outer lateral teeth, as the radula rotates over the odontophore tip (a). Lateral view of unworn articulating rachidian teeth (b). Closeup of unworn marginal cusps of a rachidian tooth (c). Central and lateral cusps maintain sharp edges after wear, extending tooth lifespan (d). Heavy wear and structural failure of rachidian tooth central and lateral cusps (e). Complete wear of rachidian tooth cusps and latero-marginal ridge (f). Rachidian tooth terminology is explained in Figure 3. Scale bars = 200 μm (a), 100 μm (b), 20 μm (c), 50 μm (d), 20 μm (e), 100 μm (f).

teeth and between teeth and the supporting radular ribbon behind it. We also show how 3D models of individual teeth can be assembled to better understand the dynamic form of the radula during drilling, as opposed to relying on single-tooth morphology. From these reconstructions, we report new features of muricid radulae, describe their variation in species representing several of the muricid subfamilies, illustrate articulation surfaces and how interactions between teeth vary during drilling, and formulate predictions about their putative functions in drilling that can be tested in the future with methods such as finite element analysis.

2 | MATERIALS AND METHODS

2.1 | Specimen preparation

Species selected for synchrotron imaging included one individual each of *Muricanthus ambiguus* (Reeve, 1845) (subfamily Muricinae) (78 mm shell length), *Thaisella kiosquiformis* (Duclos, 1832) (34 m shell length), and *Acanthais triangularis* (Blainville, 1832) (21 mm shell length) (both subfamily Rapaninae) from near Venado Island, Panama, and *Trophon geversianus* (Pallas, 1774) (subfamily Trophoninae) (35 mm shell length) from Puerto Madryn, Argentina. Radulae were isolated from full-sized, adult specimens preserved in 70% ethanol by dissecting the proboscis and dissolving the buccal mass tissues in concentrated sodium hypochlorite. Radulae were collected with forceps, washed in distilled water, snipped with forceps into three or four shorter segments, and one or two individual segments fastened cusps-side-up while still wet in the open position (lateral teeth pulled away from the rachidian as with a typical SEM mount) on the end of a 2 mm wide carbon fiber rod with polyvinyl acetate (washable Elmer's PVA glue) and allowed to air dry.

To visualize tooth wear and the radula in its functional feeding position (Figure 2), odontophores were dissected from the proboscises of several individuals of *T. geversianus*, dehydrated in a graded ethanol series, critical point dried, and attached to SEM tabs with double-sided conductive tape for SEM imaging. The smoothness of the radular membrane and the positions of interlocking teeth (e.g., Figure 2a) show that deformation of the radulae during drying was minimal.

2.2 | Scanning procedures and 3D modeling

Specimens were scanned using single propagation distance phase contrast tomography at the European Synchrotron Radiation Facility

(ESRF) in Grenoble, France using the ID19 microtomography beamline. Every specimen used the following scan parameters: 2999 angular projections collected for a 360° rotation; 0.1 ms exposure time; 360 nm^3 voxel size; 20 mm sample-to-detector distance; X-ray energy of 26.5 keV. Preparation of critical point dried specimens for SEM was the same as for synchrotron preparation except that radulae were coated with Au–Pd and mounted on stubs with double-sided conductive tape for imaging with a Philips XL 30 scanning electron microscope at the Museo Argentino de Ciencias Naturales.

Sixteen-bit Synchrotron *.tif stacks were reconstructed using "Paganin" single-distance phase retrieval algorithms (developed in-house at ID19), imported into *Avizo Lite* 9.4 (Thermo Fisher Scientific), and visually explored for mature rachidian teeth that showed no evidence of in vivo wear or post-mortem breaking during sample preparation. The scan volume was then cropped to these sections to facilitate data management. Segmentation of one tooth per species was performed semi-automatically: the "Magic Wand" tool was used initially to select the tooth volume based on grayscale intensity and then to manually remove any traces of the supporting radular membrane, mount, or mounting glue that remained attached to the teeth. Once segmented, each tooth was exported as an *.stl and brought into Geomagic Wrap 2017 (3D Systems) for smoothing and cleaning of artifacts. In one specimen (*Acanthais*), damage to the tooth was only apparent after segmentation.

Although not all muricid radulae are symmetrical (e.g., muricid subfamily Typhinae), most are, and we assumed bilateral symmetry and used paleontological protocols (Lautenschlager, 2016) to reposition and retro-deform damaged cusps of the *Acanthais* tooth in *Geomagic* and *Avizo*. Damage to the *Acanthais* specimen was addressed by creating an individual segmentation of the detached marginal cusp, which was then aligned to the body of the main tooth in Avizo and the surfaces combined in *Geomagic* using the "merge" function. The merged file was then reimported into *Avizo* where minor cracks were filled and the model was smoothed. The central cusp was repaired by selecting a "donor cusp" from an undeformed tooth from the same radula and segmenting it. The deformed central cusp from the original specimen was removed and the donor cusp aligned and merged into its place using the same methods previously applied to the marginal cusp. Segmenting artifacts in the form of ridges on the central cusp were removed by smoothing.

Rachidian base widths were measured at the widest point and are reported for individual teeth selected for segmentation. Measurements of the cusp angle from the rachidian base were taken digitally using Adobe Photoshop (version 22.4) in lateral profile. A line parallel to the radular ribbon was drawn from the apex of the tongue and projected to the equivalent position on the trailing side. An angle was then taken from this line to the tip of the cusps on the feeding side (Figure 3). Cross sections of the central cusp were taken in MeshLab v.2020.02 (Cignoni et al., 2008). A plane was defined at halfway along the trailing length of the central cusp and material distal to this plane was removed. The sectional view was oriented in the plane of the screen and traced in Photoshop. Anatomical terminology for rachidian features described previously follows Kool (1993) and Pio et al. (2014), with some new features described herein for the first time.

2.3 | Analysis of tooth–tooth contact during rotation over the odontophore

To visualize how tooth articulation surfaces interact during rotation of the radula over the odontophore, the 3D models of a segmented

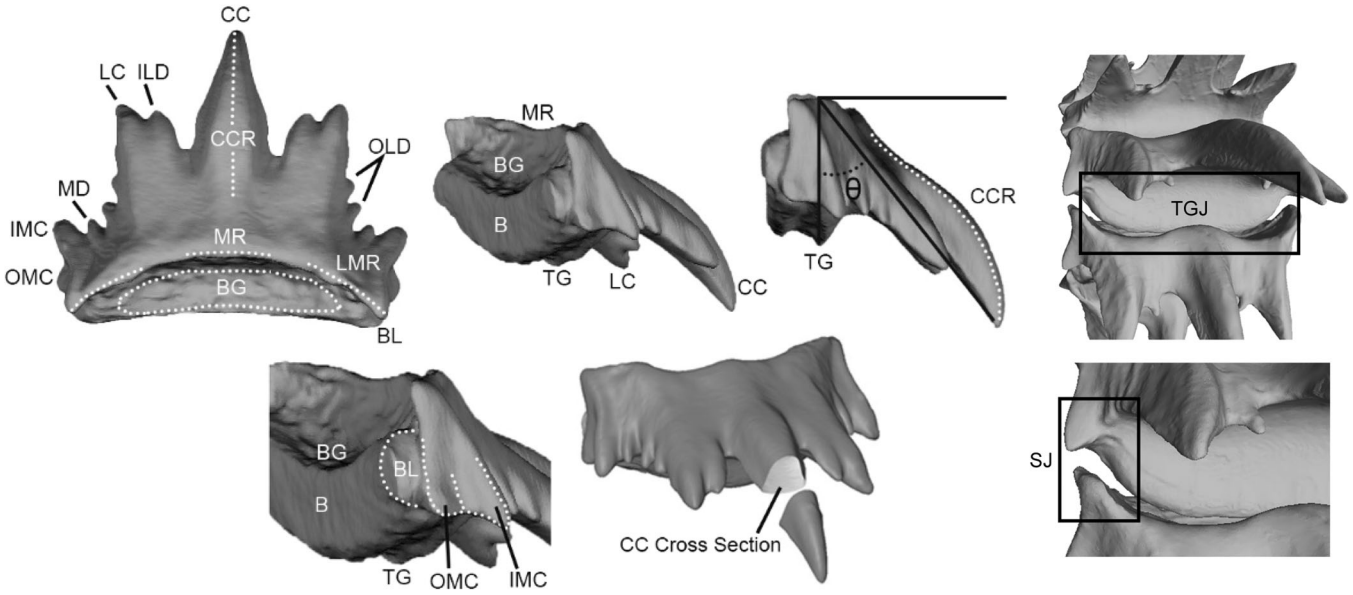

FIGURE 3 Rachidian tooth terminology. B, base; BG, basal groove; BL, basal lobe; CC, central cusp; CCR, central cusp ridge; ILD, inner lateral denticle; IMC, interior marginal cusp; LC, lateral cusp; LMR, latero-marginal ridge; MD, marginal denticle; MR, medial ridge; OLD, outer lateral denticle; OMC, outer marginal cusp; SJ, saddle joint; TG, tongue; TGJ, tongue and groove joint; θ, cusp projection angle.

tooth from *T. geversianus* and *T. kiosquiformis* were duplicated and used to reconstruct two articulated radular series of five teeth, from which cross sections and deviation maps were generated for teeth away from and at the bending plane of the odontophore. The *Remesh* function of Geomagic Wrap 2017 was used to decimate the *T. kiosquiformis* model to 500K polygons (originally 4.4M; *T. geversianus* model was 493K). For *T. geversianus*, and using Autodesk, INC., (2023), a polygonal cube was created, flattened, and positioned to represent the radular ribbon attachment and thickness, based on a reference image from the scans (Supporting Information 1). This ribbon object delineated the borders of the ventral surface of the radula that articulates with the odontophore. Within this ventral surface, a rectangular strip of polygons was selected in Geomagic Wrap 2017. A cylinder was algorithmically fit to these polygons using the *Best Fit* function and imported into *Maya* using custom MEL scripts to define the center of rotation and rotational axis *Z* of an XYZ locator object (Carney, in revision). In *Maya*, the *Y*-axis of this object was aligned to the ribbon object plane, yielding an *X*-axis that bisected the ventral articular surface. The tooth was then parented under the XYZ locator object, which in turn was translated and oriented to the world origin (0,0,0). Both the cylinder-based axes and inertial axes (via custom MATLAB script: Carney, in revision) revealed ~2° of bilateral asymmetry in the tooth, which was compensated for to align the central cusp axis to the world axis. Inertial axes were also created for the *T. kiosquiformis* tooth and used to translate and orient this model to the world origin, as well as for subsequent rotations of the other teeth in the radular series (0°, 22.5°, 45°, and 45° between each pair from left to right). ~1° of bilateral asymmetry was apparent in this tooth. However, a compensatory rotation resulted in poorer alignment between teeth in the radular series and so was not used for the final reconstruction. For *T. geversianus*, SEM images (e.g., Figure 2b) were projected onto the *Image Plane* of virtual cameras, the middle tooth of which was aligned to the 3D model and used as a reference for manually positioning four instanced duplicates of the tooth into an articulated series (two in front, two in back). Contiguity of the ribbon objects was maintained for the *T. geversianus* series, and interpenetration of the tooth models was avoided. A sagittal section was created to visualize the articulations along the axis of the central cusp for both species. Deviation maps between adjacent teeth were generated by importing the articulated series from Maya into Geomagic Wrap 2017, post-processing the model meshes (*Mesh Doctor*), flipping the normals of the anterior tooth (*Flip Normals*), and then selecting the posterior tooth for analysis (*Deviation*; with a critical angle of 45° and a maximum deviation of 20 and 10 µm for *T. geversianus* and *T. kiosquiformis*, respectively).

3 | RESULTS

3.1 | 3D model descriptions

Trophon geversianus (Pallas, 1774), Trophoninae (Figure 4a). Rachidian tooth width 203 µm. Central cusp long, narrow, gently curved along sagittal axis, with 60° angle of projection from rachidian base. Central

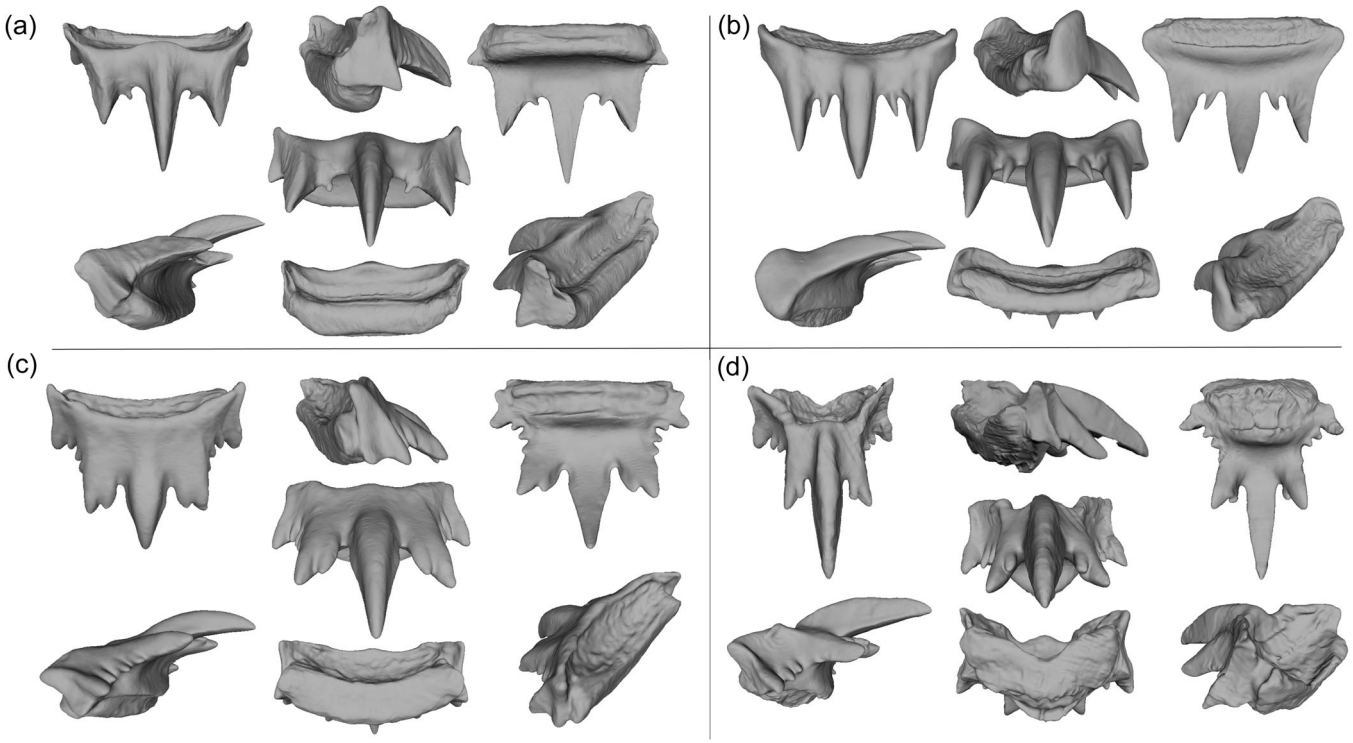

FIGURE 4 Three-dimensional renderings of rachidian teeth of *Trophon geversianus* (a), *Muricanthus ambiguus* (b), *Acanthais triangularis* (c), and *Thaisella kiosquiformis* (d). See Results text for tooth widths.

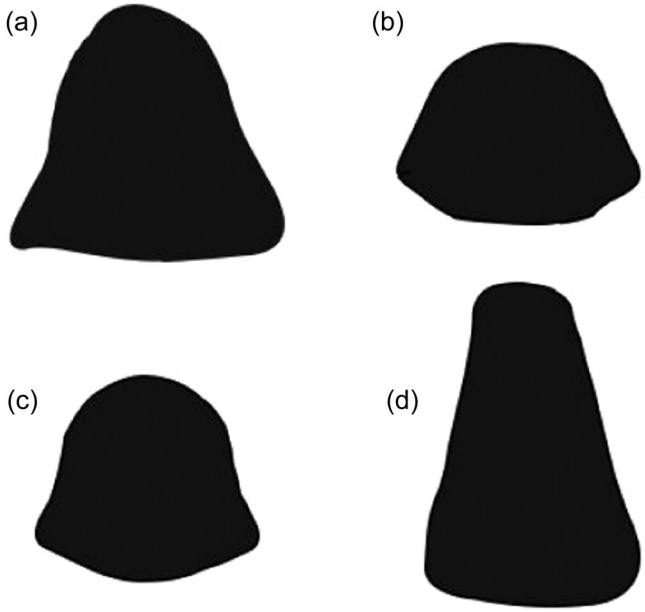

FIGURE 5 Central cusp cross sections for *Trophon geversianus* (a), *Muricanthus ambiguus* (b), *Acanthais triangularis* (c), and *Thaisella kiosquiformis* (d).

cusp cross-section triangular with rounded angles (Figure 5a), resulting in a narrow, rounded central cusp ridge. Lateral cusps short, roughly half the length of central cusp, triangular shape with wide base, bent downward (ventrally) mid-way along sagittal axis, and with 41° angle of projection from rachidian base. Inner edge of lateral cusps smooth, outer edge with three low serrations. One inner lateral denticle between central and each lateral cusp. Inner lateral denticles short, thin, sharing a common base with lateral cusp, oriented at 45° angle towards central cusp. Marginal area narrow, with one low marginal denticle. Two marginal cusps at each end of rachidian base. Inner marginal cusp short, narrow, and sharply pointed, with distal end gently curved laterally and forward (dorsally). Outer marginal cusp weakly developed as a faint ridge mid-way between inner marginal cusp and short, semi-circle-shaped basal lobe. Latero-marginal ridge narrow, restricted to marginal cusp zone. Rachidian base thick with broad, straight basal groove overlapped by prominent M-shaped medial ridge; large, rounded tongue. Medial ridge broad, rounded.

Muricanthus ambiguus (Reeve, 1845), Muricinae (Figure 4b). Rachidian tooth width 229 µm. Central cusp long, narrow, gently curved along the sagittal axis, with 43° angle of projection from rachidian base. Central cusp parabolic in cross-section (Figure 5b), resulting in a prominent, rounded central cusp ridge. Lateral cusps long, narrow, more than half the length of central cusp, gently curved along axis, with 42° angle of projection from rachidian base. The inner edge of lateral cusps with single, low serration at midlength; the outer edge smooth. One inner lateral denticle between central and each lateral cusp. Inner lateral denticles thin, free from lateral cusp, slightly recurved laterally. Marginal area narrow, smooth, arched. Marginal cusps absent. End of rachidian base rounded. Basal lobe small, semi-circular. Latero-marginal ridge high, rounded and broad, extending from marginal area to lateral cusp zone. Rachidian base thin, U-shaped with broad, shallow, U-shaped basal groove and tongue. Medial ridge narrow, low.

Acanthais triangularis (Blainville, 1832), Rapaninae (Figure 4c). Rachidian tooth width 92 µm. Central cusp is long, narrow, gently curved along sagittal axis, with 36° angle of projection from rachidian base. Central cusp cross-section is an oblate circle (Figure 5c), resulting in a broad, rounded central cusp ridge. Lateral cusps long, more than half the length of central cusp, triangular shape with wide base, slight lateral deflection, and 35° angle of projection from rachidian base. Inner edge of lateral cusps smooth, outer edge with two large, denticle-like serrations. One inner lateral denticle between central and each lateral cusp. Inner lateral denticles long, bullet-shaped, sharing a common base with lateral cusp, and slightly laterally deflected. Marginal area narrow, with one large marginal denticle. Two marginal cusps at each end of rachidian base. Inner marginal cusp long, bullet shaped, with distal end gently curved laterally. Outer marginal cusp smaller, weakly developed, in front of prominent, pointed basal lobe. Latero-marginal ridge flat-topped, broad, extending from marginal area to lateral cusp zone. Rachidian base thick with deep, U-shaped basal groove and narrow, weakly developed medial ridge; shallow, rounded tongue.

Thaisella kiosquiformis (Duclos, 1832), Rapaninae (Figure 4d). Rachidian tooth width 71 µm. Central cusp is long, narrow, with gentle curve along sagittal axis and 48° angle of projection from rachidian base. Central cusp cross-section resembles a trapezoid (Figure 5d), resulting in sharp, high central cusp ridge. Lateral cusps half the length of central cusp, with triangular shape, prominent ridge, wide base, slight lateral deflection, and 34° angle of projection from rachidian base. Inner edge of lateral cusps smooth, outer edge lacking serrations. One inner lateral denticle between central and each lateral cusp. Inner lateral denticles short, narrow, sharing a common base with lateral cusp. Marginal area wide with two large marginal denticles. Two marginal cusps at each end of rachidian base. Inner marginal cusp long, narrow, with distal end gently curved laterally. Outer marginal cusp small, weakly developed, in front of heavy, knob-like basal lobe. Latero-marginal ridge low, broad, extending from marginal area to lateral cusp zone. Rachidian base thick with a broad medial ridge and deep, bowl-shaped basal groove; narrow, rounded tongue.

3.2 | Central cusp cross-sectional and medial ridge shapes

The central cusp shafts of *Trophon*, *Muricanthus*, and *Acanthais* are bell-shaped and more or less oblate in cross-section, while the cross-section of the central cusp of *Thaisella* is more trapezoidal (Figure 5). The medial ridge ranges from a narrow and prominent ridge in *Thaisella* and *Trophon* to only a weakly developed hump in *Muricanthus* and *Acanthais* (Figure 5).

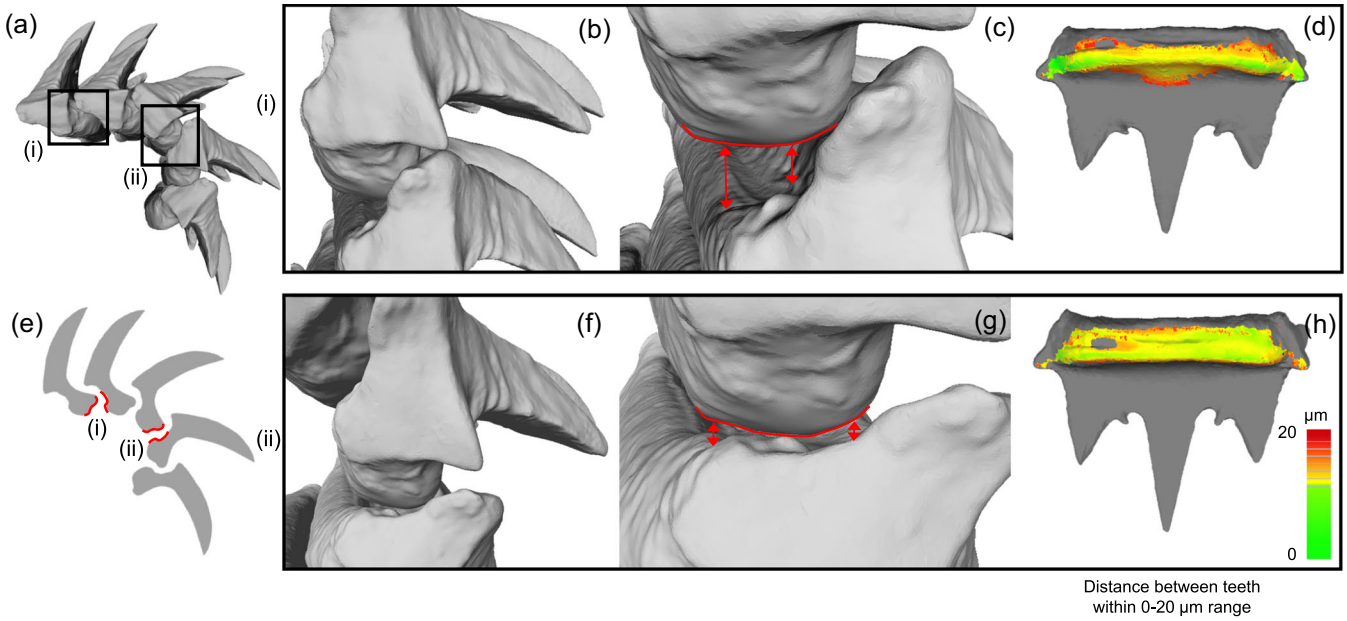

FIGURE 6 Articulated series of five duplicated tooth models of *Trophon geversianus* (a), showing tooth–tooth articulation (b, c, f, g). Sagittal section through the central cusp of the five articulated teeth, with the sigmoidal outlines of the tongue-and-groove articulation surface highlighted in red for teeth further away (i) and closer to the bending plane of the odontophore tip (ii) (e). Deviation maps illustrating distances between articulating surfaces of adjacent teeth in minimum (i) and maximum (ii) relative rotation; heat map with a linear scale of ±20 μm (d, h). Note the expansion of the tongue-and-groove articular surface and slight reduction of the saddle joint articular surfaces in (f) compared to (d).

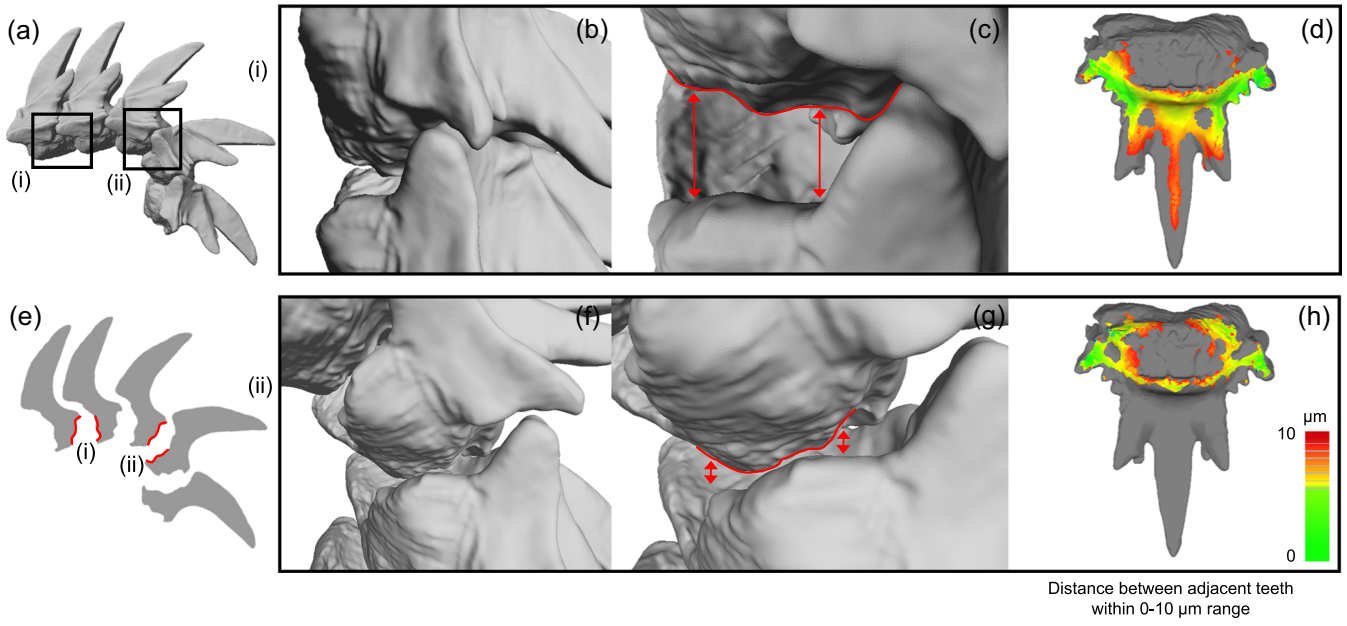

FIGURE 7 Articulated series of five duplicated tooth models of *Thaisella kiosquiformis* (a), showing tooth–tooth articulation (b, c, f, g). Sagittal section through the central cusp of the five articulated teeth, with the sigmoidal outlines of the tongue-and-groove articulation surface highlighted in red for teeth further away (i) and closer to the bending plane of the odontophore tip (ii) (e). Deviation maps illustrating distances between articulating surfaces of adjacent teeth in minimum (i) and maximum (ii) relative rotation; heat map with a linear scale of ±20 μm (d, h). Note the posterior expansion of the tongue-and-groove articular surface in (f) compared to (d), as in *Trophon geversianus*, except for a large central region of the articulation surface.

3.3 | Observations on material composition

No differences in radiodensity, which might indicate variation in internal structure, chemical composition, or mineralization, were detected within teeth or between the teeth, radular ribbon, and PVA adhesive used to mount the specimens (Supporting Information: Figure S1).

3.4 | Articulation surfaces in 3D

Scanning electron micrographs and our 3D reconstructions of the radula of *T. geversianus* show that the tongue-and-groove joint tightens posteriorly as the teeth rotate over the tip of the bending plane of the odontophore, even as the angle between central cusps of adjacent teeth increases (Figures 2a–f and 6). Conversely, the saddle joint at the marginal cusps becomes more open for *T. geversianus*. For *T. kiosquiformis*, the tongue-and-groove joint also tightens posteriorly for teeth near the bending plane of the odontophore, but the extent of tightening across the tongue is much less due to the much greater depth of the basal groove in *T. kiosquiformis* (Figure 7). Distances between articulation surfaces of the saddle joints in *T. kiosquiformis* show little change in teeth further from and closer to the bending plane of the odontophore.

4 | DISCUSSION

4.1 | Major results

Our synchrotron scans reveal the complete 3D morphology of the muricid rachidian teeth for the first time, including two previously undescribed types of articulation surfaces: (1) a tongue-and-groove system that articulates adjacent tooth bases as a hinge joint and (2) two saddle joints, one at each end of the rachidian tooth formed by an arched shoulder (latero-marginal ridge) on the posterior tooth that fits within a notch in the adjacent, anterior tooth. Our study also reveals substantial variation between species in the shapes of these articulation surfaces and how they are formed (Figure 4).

The tongues of these tongue-and-groove joints vary most obviously in length but also in degree of curvature, the presence of ridges, and width of the attachment zone between the rachidian tooth and the backing radular membrane. The corresponding groove varies from a rectanglar depression that is open on one side to a deep bowl-shaped depression. Variation in the saddle joint notch is determined primarily by those features that create the notch. The notch is formed by the angle between two marginal cusps in some species, while in others it forms between the lateral cusp and basal lobe, the marginal cusp and basal lobe, or the outer marginal cusp and the basal lobe (Figure 4; also Pio et al., 2014: figs. 1 and 3). There is also variation in the position of the latero-marginal ridge (part of the adjacent tooth that fits within the saddle joint) between species, which can form above each marginal cusp or each lateral cusp or span both (Figure 4; Herbert et al., 2007, 2015; Pio et al., 2014).

Although Carriker et al. (1974) did not describe specific articulation types, they hypothesized that "basal support" in the muricid radula might be an adaptation for dispersing forces from violent impacts during predatory shell drilling across multiple rachidian teeth, thereby preventing stress buildup within any individual tooth. Experimental evidence for force dispersion by tooth–tooth contact has since been demonstrated in other mollusks, including chitons and paludomid gastropods (Krings, Brütt, et al., 2022; Krings, Kovalev, Gorb, 2021a, 2021b). Our 3D reconstructions of 5-tooth rachidian series for *T. geversianus* and *T. kiosquiformis* reveal that the articulation surfaces of the tongue-and-groove joint (Figures 6e and 7e) become increasingly parallel (i.e., improved fit) as teeth approach the striking tip of the odontophore. This may represent a unique type of joint that has not yet been described. We hypothesize that if improved fit of the tongue-and-groove surfaces of teeth at the striking tip of the odontophore exists in vivo, it would allow for tooth–tooth contact to increase during drilling, along with increased potential for force dispersion between the striking tooth and adjacent teeth. Thus, Carriker et al.'s (1974) hypothesis that tooth–tooth contact is capable of dispersing impact forces during drilling is supported by our observations, but our study goes further in showing how tooth fit and potential for force dispersion improve at the striking tip of the odontophore. Future should explore how tooth–tooth fit over the odontophore varies across the Muricidae and whether there is evidence for adaptive improvement, that is, directional trends from more basal to more recently evolved lineages.

Well-developed articulating bases are common but not ubiquitous across the Muricidae. The muricine *M. ambiguus*, for example, has a relatively shallow tongue-and-groove hinge joint (Figure 4b), and the anterior end of the saddle hinge is formed by a shallow depression between the lateral cusp and base endpoint. In contrast, the rapanine *T. kiosquiformis* has a deep tongue-and groove hinge and a saddle hinge developed as a sharp notch between two marginal cusps (Figure 4d). In general, simpler and more weakly developed articulating bases are found in the subfamilies Muricinae and Haustrinae; variable complexity and development are found in the Rapaninae, Ergalataxinae, Muricopsinae, and Trophoninae; and complex and strongly developed articulating bases are found in the Ocenebrinae (Herbert et al., 2007, 2015; Pio et al., 2014). Since the Muricinae predates all other subfamilies in the fossil record by at least 20 million years (Merle, 2012; Vermeij & Carlson, 2000), we propose that more complex tooth articulation was absent in earliest muricids and evolved later as drilling increased in frequency as a mode of attack, as prey shells thickened and drilling times increased, and/or as interactions between drillers and their own predators intensified selection for more efficient drilling. Conversely, relaxation in selection for traits that reduce stress and strain on teeth is expected in lineages where the use of drilling has given way to faster, non-drilling feeding modes, such as use of toxins, shell chipping, and parasitism (Dietl & Herbert, 2005; Herbert, 2004; Herbert et al., 2007, 2009, 2016; Paul et al., 2015; Pio et al., 2014). This

hypothesis would be most productively explored in subfamilies with the greatest diversity of articulation surfaces, well-resolve phylogenies, and abundant feeding and dietary observations (e.g., Rapaninae).

Testing these hypotheses rigorously would require advances over previous work, which have tended to focus on how radular teeth deform and distribute stresses and strain in isolation during feeding (Krings et al., 2020; Lee et al., 2023; Van der Wal et al., 2000). While studying tooth performance in isolation can give valuable insight into the structural performance of tooth morphology, interactions between adjacent tooth bases must be factored in in studies of the muricid radula. Krings, Marcé-Nogué, et al. (2021) modeled a section of a gastropod radula comprising multiple teeth embedded within the radula ribbon. This approach permits some understanding of how different teeth respond to the same loading scenario. However, the close tooth arrangement and highly dynamic motion of the radula as it passes over the odontophore tip in muricids may require use of more computationally-complex, nonlinear, large-displacement models with well-defined, non-penetrating contact surfaces to fully resolve between-tooth strains (see Marcé-Nogué, 2022 for an in-depth discussion of these issues).

4.2 | Alternative explanations for saddle and tongue-and-groove joints

An alternative explanation for tooth–tooth articulation features of gastropod radulae is that they counteract bending and torsional forces along the radula during feeding by holding teeth in place (Hickman, 1980, 1984). This explanation could apply to saddle joints in some muricid species because of the way marginal cusps wrap laterally around the adjacent tooth (e.g., *T. kiosquiformis*: Figure 7f,g). This is supported by (1) the fact that the saddle joints of *T. geversianus* are maximally open (least contact) when teeth are at the striking tip of the odontophore, unlike its tongue-and-groove joint; and (2) observations of wear of the latero-marginal ridge on teeth in several specimens of *T. geversianus* (Figure 2d–f). The latter type of wear can only be explained by tooth–tooth interactions since the latero-marginal ridge does not face the prey shell surface.

An unexpected finding of our research was the large, circular area of no contact (a large open space) in the center of the tongue-and-groove joint articulation surface of *T. kiosquiformis*, even when teeth are rotated into feeding position and the tongue and groove fit is tightest (Figure 7h). This open space is created by a deep, basin-like groove and short tongue in *T. kiosquiformis*. The function of this deep basin is unknown, but another rapanine, *Plicopurpura patula*, has a similar deep, basin-like groove that opens into an open slit down the center of a long, hypodermic-needle-like central cusp (Figure 8; also Kool, 1993: fig. 17e). Since hypodermic-needle-like teeth are associated with toxin delivery in other predatory gastropods (Puillandre et al., 2017), basin-like depressions that open into the needle plausibly store toxins. Basin-like grooves with poor tongue-and-groove surface articulation in other species could serve a similar function. This hypothesis is speculative but mentioned as there are alternatives to purely biomechanical explanations for tooth shape in the Muricidae.

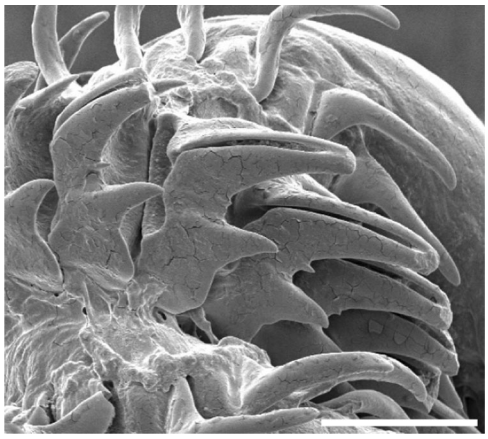

FIGURE 8 Radula of the rapanine muricid *Plicopurpura patula* showing deep, basin-like groove of the rachidian base that connects to an open slit down the center of the central cusp. Scale bar = 100 μm.

4.3 | Distribution of articulating rachidian bases in the Neogastropoda

Rachidian bases with articulating tongue-and-groove or saddle joints are either completely absent or poorly developed in almost all other Neogastropoda outside of the Muricidae, including Buccinoidea (Fedosov & Kantor, 2012; Harasewych, 2018), Olivoidea (Kantor & Bouchet, 2007; Kantor et al., 2017), Conoidea (Kantor et al., 2018), Mitroidea (Fedosov et al., 2015, 2017), and Turbinelloidea (Kantor et al., 2001). Most of these neogastropods use the radula for piercing, raking, and scooping soft prey tissues rather than drilling through hard shell (Taylor, 1998). Exceptions include a small number of species of Volutoidea (e.g., *Cysticus* sp.: Fedosov et al., 2019: fig. 4c,d) and Turbinelloidea (*Ceratoxancus* spp: Kantor & Bouchet, 1997; *Cyomesus chaunax* Harasewych, 1987: fig. 20) that have tooth–tooth contact, shallow- to moderately-deep tongue-and-groove articulation, and a present but weakly-developed saddle joint (i.e., latero-marginal ridge bounded by one cusp). Kantor and Bouchet (1997, pp. 119–20) speculated that at least one of these, *Ceratoxancus basileus*, drills shelled prey based on SEMs of the radula showing rachidia worn flat to the base (Kantor & Bouchet, 1997: fig. 3b). Other species of *Ceratoxancus* have been found to use a labral spine on the shell's aperture to wedge open large bivalve prey (Kantor & Bouchet, 1997), a mode of attack also used by some muricids in combination with drilling (Vermeij, 2001). Given current knowledge of family-level phylogenetic relationships among neogastropods (e.g., Fedosov et al., 2015), these sporadic occurrences of articulating tooth bases outside the Muricidae probably represent independent origins.

4.4 | Biomechanics of the rachidian cusps

4.4.1 | Cusp shape

Our 3D scans illustrate morphological variation of rachidian cusps, ridges, and denticles across the family. Muricid rachidia usually have three major cusps, including a long central cusp flanked on each side by one lateral cusp (Herbert et al., 2007). Cusps come to a sharp point distally, which helps generate fracture-inducing stresses in the prey shell. The cusp shaft functions as a cantilevered beam that is loaded in bending when it contacts the prey shell. Stresses developed in a beam under bending are dependent on both the cross-sectional shape of the beam (the second moment of area) and the bending moments it experiences, which are themselves dependent on the length and curvature of the beam, and the magnitude and direction of the loading force. Length and curvature of the cusps vary widely between species and within species during ontogeny (Herbert et al., 2007, 2015; Pio et al., 2014).

Cusp cross-sectional shapes vary between species in the Muricidae, potentially affecting performance. Although a trapezoidal cross section results in a blunter cusp tip and, thus, potentially lower fracture-inducing stresses on the prey shell, Euler–Bernoulli beam theory predicts that under bending loads, such a cross-section will be comparatively stronger in bending in the antero-posterior direction. As this is the dominant loading direction during feeding, we predict that the trapezoidalcross-sectional cusp shape of *T. kiosquiformis* should better resist bending stresses in the shaft relative to bell-shaped cross-sectional shapes.

Curvature of the cusp along its main axis is also important, because forces from drilling produce higher moment arms (and therefore stresses) in a straight cusp than in a curved one. Using two-dimensional (2D) finite element analysis, Van der Wal et al. (2000) showed that a curved cusp shifts stresses away from the tooth tip and towards the leading (flatter) edge of the base compared to a straight cusp. The curvature and cross-sectional shapes of the cusp shafts may therefore covary to minimize bending stresses experienced during feeding. In all species, the leading edge of the cross-section is wider than the trailing edge, which may act to compensate for the effects of shaft curvature.

The medial ridge at the base of the central cusp is another interesting source of variation in the species studied. Manual manipulation of 3D prints of the teeth suggests that even the most prominent medial ridge is unlikely to come in to contact with the tongue of the trailing tooth to prevent over-rotation. Instead, we suggest that the presence of the ridge acts to increase the antero-posterior height of the cusp at the base of the shaft, increasing the second moment of area (and thus the resistance to bending) in this direction. We also note from published SEM studies that the relative size and shape of this ridge changes throughout ontogeny, with younger snails tending to have a sharper and more prominent ridge (Herbert et al., 2007, 2015; Pio et al., 2014). Juvenile snails also tend to drill more than their adult counterparts (Herbert et al., 2007, 2016), and therefore might be expected to have tooth shapes that reflect this mode of feeding, or that their teeth need to be more efficient to compensate for their comparatively small size. If the medial ridge is an adaptation for resistance to bending, then this ontogenetic difference is interesting, as paedomorphosis has been observed in muricid radulae before, and implies that heterochronic shifts could be the mechanism by which drilling evolved in this group (Herbert et al., 2007, 2015).

4.4.2 | Changes in cusp shape and length with wear

Tooth wear during drilling alters cross-sectional shapes, lengths, and curvature of the central and lateral cusps (Figure 2), although the effect of wear on drilling performance is unknown. Hickman (1980) points out that the unworn state of a tooth may not represent its most efficient functional shape. The most efficient shape for drilling may instead only arise after some wear has taken place. Recognition of this context may offer further insight on the curvature of radular cusp shafts. During feeding, the radula can be thought of as a cutting tool with rake and clearance angles (Van der Wal et al., 2000). An efficient tool requires these angles to be positive, and, in particular, that the clearance angle stay above zero to allow the tool purchase on the worked surface. Assuming that the animal maintains a consistent feeding stroke, the curvature of the shaft allows a positive clearance angle to remain as the cusp wears. Wear patterns in *T. geversianus* (Figure 2) suggest that cusps may have distinct mechanical properties between the leading and trailing edges that would cause them to be self-sharpening, although this has not yet been studied. Extreme cusp wear eventually eliminates the cusps altogether but brings the smaller denticles between the cusps and denticles into contact with the prey shell, potentially extending the life of the tooth as a drilling tool (Figure 2).

4.5 | Material properties of muricid radulae

Muricid snails build their radulae from chitin, with various degrees of tanning or mineralization by calcium, silica, strontium, and other trace metals (Carriker & Van Zandt, 1972; Hickman, 1980; Tyler & Schiffbauer, 2012). Tomographic data from the four specimens studied here suggest that the muricid rachidian tooth is homogeneous in composition, with no distinct layers of different elemental composition (e.g., metal), as previously observed in studies of chitons (Wealthall et al., 2005; Weaver et al., 2010). We infer that the muricid rachidian teeth are mostly organic with low mineralization due to its similarity under X-rays to both the radular ribbon and the PVA mounting glue (Supporting Information: 1). A caveat in this finding is that synchrotron images cannot easily detect ultrastructural heterogeneities when there is no change in material (Wealthall et al., 2005) or when they are below the 360 nm resolution of the synchrotron (e.g., Lu & Barber, 2012; Tyler & Schiffbauer, 2012; Wang et al., 2014; Weaver et al., 2010).

5 | CONCLUSIONS

Padilla (2003) outlines three main areas in which to focus future studies of radular form and function, specifically: the quantification of morphology, explicit tests of function, and efforts towards a synthesis of the two. While the small size of the radula has historically presented several challenges in the imaging and functional study of this organ, many of these challenges can now be overcome in light of technological advances in imaging and the field of functional morphology. In any study of functional morphology, a reasonable geometric model of the morphology concerned must first be obtained. Although SEMs offer excellent spatial resolution, they are still 2D images. Synchrotron imaging allows us to capture detailed three-dimensional (3D) representations of radular morphology (see also Kruta et al., 2015 for an ammonoid example), offering the chance to observe several new features. Once obtained, these models may then be used in advanced downstream analyses that address each of Padilla (2003), focal concerns.

The field of geometric morphometrics has advanced significantly since 2003 (Adams et al., 2013), allowing for the detailed quantification and analysis of organismal form in three dimensions. A potential limitation of landmark-based geometric morphometrics when applied to the radula is a lack of homologous landmark points across taxa; however, advances in the use of "homology-free" landmarks (e.g., Boyer et al., 2015) mean that geometric morphometrics is a viable tool for the study of this system. In addition to capturing detailed 3D data, synchrotron scanning also has a dramatically higher rate of throughput than other tomographic methods, meaning that the large sample sizes necessary for geometric morphometrics studies may be obtained. The main rate-limiting steps are gaining access to a synchrotron facility and the time taken to segment the tomographic data.

In vivo and ex vivo experiments on radula function are difficult to conduct, owing to the radula's small size (although see Carriker et al., 1974; Krings et al., 2019; Padilla, 1985, 1989). Our synchrotron approach can overcome these limitations in two creative ways. The first is that, once segmented, radular teeth are represented as computer surface files suitable for up-scaled 3D printing. This allows for physical models to be produced for in vitro experimental work (e.g., Krings, Karabacak, et al., 2021). The second, and more versatile, implication of this is the potential for in silico functional testing using finite element analysis (FEA; reviewed in Bright, 2014) and multibody dynamics analysis (MDA; reviewed in Curtis, 2011). The use of deductive and inductive FEA within and between taxa allows specific hypotheses about the stress performance of traits to be tested (Rayfield, 2007). MDA can test hypotheses on likely ranges of motion, and thanks to its collision-detection capabilities, investigate tooth–tooth interactions and the potential for disarticulation. Critically, FEA and MDA can be combined with one another (e.g., Lautenschlager et al., 2018) or with geometric morphometrics (Polly et al., 2016) to build a comprehensive analytical framework in which to interrogate the links between function and form in an evolutionary context. This combination of methodologies therefore allows us to untangle a key problem identified in studies of snail radulae by Hickman (1980): that not all features are necessarily adaptive (indeed, such thinking is problematic across all taxa; see Lauder, 1995).

AUTHOR CONTRIBUTIONS

Gregory S. Herbert: Conceptualization; writing—original draft; writing—review & editing; resources; methodology; data curation; supervision; visualization; funding acquisition; project administration; investigation. **Stephen A. Hill**: Visualization; writing—review & editing; investigation. **Maria Jose Pio**: Data curation; methodology; writing—review & editing; visualization; conceptualization; investigation. **Ryan Carney**: Conceptualization; data curation; methodology; investigation; formal analysis; project administration; writing—original draft; writing—review & editing; visualization; supervision. **Amber Carlson**: Visualization; writing— review & editing; investigation. **Elis Newham**: Data curation; methodology; writing—review & editing. **Jen A. Bright**: Conceptualization; writing—review & editing; writing—original draft; project administration; supervision; visualization; resources; methodology; data curation; software; investigation; formal analysis; funding acquisition; validation.

ACKNOWLEDGMENTS

The authors thank the University of South Florida for travel grants to G. S. H. to conduct field work in Panama and Argentina; Jerry Harasewych and Gregorio Bigatti for logistical support of lab and field work in Panama and Argentina, respectively; Vincent Fernandez, Pamela Gill, and Julia Schultz for assistance with synchrotron scanning; Fabián Tricarico for assistance with Scanning Electron Microscopy; Philip Morris for help with Avizo; and two reviewers for helpful comments.

CONFLICT OF INTEREST STATEMENT

The authors declare no conflict of interest.

DATA AVAILABILITY STATEMENT

The data that support the findings of this study are openly available in Digital Commons University of South Florida at https://digitalcommonsdata.usf.edu/drafts/d5p97fcx3s.

ORCID

Gregory S. Herbert http://orcid.org/0000-0001-7312-6147
Stephen A. Hill http://orcid.org/0000-0001-8124-1735

PEER REVIEW

The peer review history for this article is available at https://www.webofscience.com/api/gateway/wos/peer-review/10.1002/jmor.21633.

REFERENCES

Adams, D. C., Rohlf, F. J., & Slice, D. E. (2013). A field comes of age: Geometric morphometrics in the 21st century. *Hystrix, the Italian Journal of Mammalogy*, *24*, 7–14.

Autodesk, I. N. C. (2023). Maya. Retrieved from https:/autodesk.com/maya

Boyer, D. M., Puente, J., Gladman, J. T., Glynn, C., Mukherjee, S., Yapuncich, G. S., & Daubechies, I. (2015). A new fully automated approach for aligning and comparing shapes. *The Anatomical Record*, *298*, 249–276.

Bright, J. A. (2014). A review of paleontological finite element models and their validity. *Journal of Paleontology*, *88*, 760–769.

Carney, R. M. (in revision). Topological coordinate systems: A joint surface approach for comparative skeletal analysis and scientific motion transfer.

Carriker, M. R. (1981). Shell penetration and feeding by naticacean and muricacean predatory gastropods: A synthesis. *Malacologia*, *20*, 403–422.

Carriker, M. R., & Gruber, G. L. (1999). Uniqueness of the gastropod accessory boring organ (ABO): Comparative biology, an update. *Journal of Shellfish Research*, *18*, 579–595.

Carriker, M. R., & Schaadt, J. G. (1973). Predatory behavior of the shell-boring snail *Urosalpinx cinerea*: A sound, color, motion picture. MBL Woods Hole. Available from Smithsonian Institution Archives, Accession 08-005, Melbourne R. Carriker Papers.

Carriker, M. R., Schaadt, J. G., & Peters, V. (1974). Analysis by slow-motion picture photography and scanning electron microscopy of radular function in *Urosalpinx cinerea follyensis* (Muricidae, Gastropoda) during shell penetration. *Marine Biology*, *25*, 63–76.

Carriker, M. R., & Van Zandt, D. (1972). Predatory behavior of a shell-boring muricid gastropod. In H. E. Winn & B. L. Olla (Eds.), *Behavior of marine animals: Current perspectives in research, Vol. 1, invertebrates* (pp. 157–244). Plenum Press.

Cignoni, P., Callieri, M., Corsini, M., Dellepiane, M., Ganovelli, F., Ranzuglia, G. (2008). *MeshLab: An open-source mesh processing tool*. Sixth Eurographics Italian Chapter Conference, 129-136.

Cunningham, J. A., Rahman, I. A., Lautenschlager, S., Rayfield, E. J., & Donoghue, P. C. J. (2014). A virtual world of paleontology. *Trends in Ecology & Evolution*, *29*, 347–357.

Curtis, N. (2011). Craniofacial biomechanics: An overview of recent multibody modelling studies. *Journal of Anatomy*, *218*, 16–25.

Dietl, G. P., & Herbert, G. S. (2005). Influence of alternative shell-drilling behaviours on attack duration of the predatory snail, *Chicoreus dilectus*. *Journal of Zoology*, *265*, 201–206.

Donoghue, P. C. J., Bengtson, S., Dong, X., Gostling, N. J., Huldtgren, T., Cunningham, J. A., Yin, C., Yue, z, Peng, F., & Stampanoni, M. (2006). Synchrotron x-ray tomographic microscopy of fossil embryos. *Nature*, *442*, 680–683.

Fedosov, A., Puillandre, N., Kantor, Y., & Bouchet, P. (2015). Phylogeny and systematics of mitriform gastropods (Mollusca: Gastropoda: Neogastropoda): Phylogeny of Mitriform gastropods. *Zoological Journal of the Linnean Society*, *175*, 336–359.

Fedosov, A. E., Caballer Gutierrez, M., Buge, B., Sorokin, P. V., Puillandre, N., & Bouchet, P. (2019). Mapping the missing branch on the neogastropod tree of life: Molecular phylogeny of marginelliform gastropods. *Journal of Molluscan Studies*, *85*, 439–451.

Fedosov, A. E., & Kantor, Y. I. (2012). A new species and genus of enigmatic turriform Fasciolariidae from the Central Indo-Pacific (Gastropoda: Neogastropoda). *Archiv für Molluskenkunde International Journal of Malacology*, *141*, 137–144.

Fedosov, A. E., Puillandre, N., Herrmann, M., Dgebuadze, P., & Bouchet, P. (2017). Phylogeny, systematics, and evolution of the family Costellariidae (Gastropoda: Neogastropoda). *Zoological Journal of the Linnean Society*, *179*, 541–626.

Fujioka, Y. (1985). Seasonal aberrant radular formation in *Thais bronni* (Dunker) and *T. clavigera* (Küster) (Gastropoda: Muricidae). *Journal of Experimental Marine Biology and Ecology*, *90*, 43–54.

Harasewych, M. G. (1987). A revision of the genus *Benthovoluta* with notes on the evolution of the subfamily Ptychatractinae (Prosobranchia: Turbinellidae). *The Nautilus*, *101*, 166–181.

Harasewych, M. G. (2018). The anatomy of *Tudicla spirillus* (Linnaeus, 1767) and the relationships of the Tudiclidae (Gastropoda: Neogastropoda). *The Nautilus*, *132*, 35–44.

Harding, J. M., Gera, S. M., & Mann, R. (2008). Radula morphology in veined rapa whelks, *Rapana venosa* (Valenciennes, 1846 (Gastropoda: Muricidae) from Chesapeake Bay, USA). *The Nautilus*, *122*, 217–227.

Hemingway, G. T. (1975). Functional morphology of feeding in the predatory whelk, *Acanthina spirata* (Gastropoda: Prosobranchia). *Bulletin of the American Malacological Union, Inc*. (pp. 64–65) (Abstract).

Herbert, G. S. (2004). Observations on diet and mode of predation in *Stramonita biserialis* (Gastropoda: Muricidae) from the northern Gulf of California. *Festivus*, *36*, 41–45.

Herbert, G. S., Dietl, G. P., Fortunato, H., Simone, L. R., & Sliko, J. L. (2009). Extremely slow feeding in a tropical drilling ectoparasite, *Vitularia salebrosa* (King and Broderip, 1832) (Gastropoda: Muricidae), on molluscan hosts from Pacific Panama. *The Nautilus*, *123*(3), 121–136.

Herbert, G. S., Merle, D., & Gallardo, C. S. (2007). A developmental perspective on evolutionary innovation in the radula of the predatory Neogastropod family Muricidae. *American Malacological Bulletin*, *23*, 17–32.

Herbert, G. S., Pio, M. J., Pastorino, G., Harasewych, M. G., Kantor, Y. I., Lamy, D., & Pointier, J.-P. (2015). Morphological development of the radula of four species of the Neogastropod family Muricidae. *Malacologia*, *58*, 323–336.

Herbert, G. S., Whitenack, L. B., & McKnight, J. Y. (2016). Behavioural versatility of the giant murex *Muricanthus fulvescens* (Sowerby, 1834) (Gastropoda: Muricidae) in interactions with difficult prey. *Journal of Molluscan Studies*, *82*(3), 357–365.

Hickman, C. S. (1980). Gastropod radulae and the assessment of form in evolutionary paleontology. *Paleobiology*, *6*, 276–294.

Hickman, C. S. (1984). Implications of radular tooth-row functional integration for archaeogastropod systematics. *Malacologia*, *25*, 43–160.

Huxley, T. H. (1853). II. On the morphology of the cephalous mollusca, as illustrated by the anatomy of certain heteropoda and pteropoda collected during the voyage of HMS "Rattlesnake" in 1846-50. *Philosophical Transactions of the Royal Society of London*, *143*, 29–65.

Kabat, A. (1990). Predatory ecology of naticid gastropods with a review of shell boring predation. *Malacologia: International Journal of Malacology*, *32*, 155–193.

Kantor, Y. I., Fedosov, A., & Puillandre, N. (2018). New and unusual deep-water Conoidea revised with shell, radula and DNA characters. *Ruthenica, Russian Malacological Journal*, *28*, 47–82.

Kantor, Y. I., & Bouchet, P. (1997). The anatomy and systematics of *Ceratoxancus*, a genus of deep-water Ptychatractinae (Gastropoda: Turbinellidae) with labral spine. *The Veliger*, *40*, 101–120.

Kantor, Y. I., & Bouchet, P. (2007). Out of Australia: *Belloliva* (Neogastropoda: Olividae) in the Coral Sea and New Caledonia. *American Malacological Bulletin*, *22*, 27–73.

Kantor, Y. I., Bouchet, P., & Oleinik, A. (2001). A revision of the recent species of *Exilia*, formerly *Benthovoluta* (Gastropoda: Turbinellidae). *Ruthenica*, *11*, 81–136.

Kantor, Y. I., Fedosov, A. E., Puillandre, N., Bonillo, C., & Bouchet, P. (2017). Returning to the roots: Morphology, molecular phylogeny and classification of the Olivoidea (Gastropoda: Neogastropoda). *Zoological Journal of the Linnean Society*, *180*, 493–541.

Kool, S. P. (1993). Phylogenetic analysis of the Rapaninae (Neogastropoda; Muricidae). *Malacologia*, *35*, 155–259.

Krings, W., Brütt, J.-O., & Gorb, S. N. (2022). Ontogeny of the elemental composition and the biomechanics of radular teeth in the chiton *Lepidochitona cinerea*. *Frontiers in Zoology*, *19*, 19. https://doi.org/10.1186/s12983-022-00465-w

Krings, W., Faust, T., Kovalev, A., Neiber, M. T., Glaubrecht, M., & Gorb, S. (2019). In slow motion: Radula motion pattern and forces exerted to the substrate in the land snail *Cornu aspersum* (Mollusca, Gastropoda) during feeding. *Royal Society Open Science*, *6*, 190222. https://doi.org/10.1098/rsos.190222

Krings, W., Karabacak, H., & Gorb, S. N. (2021). From the knitting shop: The first physical and dynamic model of the taenioglossan radula

(Mollusca: Gastropoda) aids in unravelling functional principles of the radular morphology. *Journal of the Royal Society Interface*, *18*, 20210377. https://doi.org/10.1098/rsif.2021.0377

Krings, W., Kovalev, A., & Gorb, S. N. (2021a). Influence of water content on mechanical behaviour of gastropod taenioglossan radulae. *Proceedings of the Royal Society B*, 288, 20203171.

Krings, W., Kovalev, A., & Gorb, S. N. (2021b). Collective effect of damage prevention in the taenioglossan radular teeth is related to the ecological niche in Paludomidae (Gastropoda: Cerithioidea). *Acta Biomaterialia*, *135*, 458–472.

Krings, W., Marcé-Nogué, J., & Gorb, S. N. (2021). Finite element analysis relating shape, material properties, and dimensions of taenioglossan radular teeth with trophic specialisations in Paludomidae (Gastropoda). *Scientific Reports*, *11*, 22775.

Krings, W., Marcé-Nogué, J., Karabacak, H., Glaubrecht, M., & Gorb, S. N. (2020). Finite element analysis of individual taenioglossan radular teeth. *Acta Biomaterialia*, *115*, 317–332.

Krings, W., Matsumura, Y., Brütt, J.-O., & Gorb, S. N. (2022). Material gradients in gastropod radulae and their biomechanical significance: A combined approach on the paludomid *Lavigeria grandis*. *The Science of Nature*, *109*, 52. https://doi.org/10.1007/s00114-022-01822-9

Kruta, I., Landman, N. H., & Tanabe, K. (2015). Ammonoid radula. In C. Klug, D. Korn, K. De Baets, I. Kruta, & R. Mapes (Eds.), *Ammonoid paleobiology: From anatomy to ecology*. Topics in Geobiology (Vol. 43). Springer. https://doi.org/10.1007/978-94-017-9630-9_11

Lauder, G. V. (1995). On the inference of function from structure. In J. J. Thomason (Ed.), *Functional morphology in vertebrate paleontology* (pp. 1–18). Cambridge University Press.

Lautenschlager, S. (2016). Reconstructing the past: Methods and techniques for the digital restoration of fossils. *Royal Society Open Science*, *3*, 160342. https://doi.org/10.1098/rsos.160342

Lautenschlager, S., Gill, P. G., Luo, Z.-X., Fagan, M. J., & Rayfield, E. J. (2018). The role of miniaturization in the evolution of the mammalian jaw and middle ear. *Nature*, *561*, 533–537.

Lee, J.-E., Connolly, J., Yang, W., Freychet, G., Wang, T., Herrera, S. A., Murata, S., Dasika, P. S., Montroni, D., Pohl, A., Zhu, C., Zhernenkov, M., Wuhrer, R., Sheppard, L., Nemoto, M., Arakaki, A., Zavattieri, P., & Kisailus, D. (2023). Fibrous anisotropy and mineral gradients within the radula stylus of chiton: Controlled stiffness and damage tolerance in a flexible biological composite. *Journal of Composite Materials*, *57*, 565–574.

Lu, D., & Barber, A. H. (2012). Optimized nanoscale composite behaviour in limpet teeth. *Journal of the Royal Society Interface*, *9*, 1318–1324.

Marcé-Nogué, J. (2022). One step further in biomechanical models in palaeontology: A nonlinear finite element analysis review. *PeerJ*, *10*, e13890. https://doi.org/10.7717/peerj.13890

Merle, D. (2012). *Les Gastéropodes cénozoïques: caractères, radiations et biodiversité. Mémoire d'habilitation à diriger des recherches (HDR)*, (p. 200).

Morton, B., & Chan, K. (1997). First report of shell boring predation by a member of the Nassariidae (Gastropoda). *Journal of Molluscan Studies*, *63*, 476–478.

Padilla, D. K. (1985). Structural resistance of algae to herbivores. *Marine Biology*, *90*, 103–109.

Padilla, D. K. (1989). Algal structure defenses: Form and calcification in resistance to tropical limpets. *Ecology*, *70*, 835–842.

Padilla, D. K. (2003). Form and function of radular teeth of herbivorous molluscs: Focus on the future. *American Malacological Bulletin*, *18*, 163–168.

Paul, S., Herbert, G. S., & Dietl, G. P. (2015). Predator-induced edge-drilling behaviour of *Chicoreus dilectus* (Gastropoda: Muricidae). *Journal of Molluscan Studies*, *81*(2), 233–237.

Pio, M. J., Herbert, G. S., & Pastorino, G. (2014). Developmental origins of complex radular characters in the Muricidae: The bifid rachidian edge. *Invertebrate Biology*, *133*(1), 64–73.

Polly, P. D., Stayton, C. T., Dumont, E. R., Pierce, S. E., Rayfield, E. J., & Angielczyk, K. D. (2016). Combining geometric morphometrics and finite element analysis with evolutionary modeling: Towards a synthesis. *Journal of Vertebrate Paleontology*, *36*, e1111225.

Ponder, W. F., & Taylor, J. D. (1992). Predatory shell drilling by two species of *Austroginella* (Gastropoda: Marginellidae). *Journal of Zoology*, *228*(2), 317–328.

Puillandre, N., Fedosov, A. E., & Kantor, Y. I. (2017). Systematics and evolution of the Conoidea. In A. Malhotra (Ed.), *Evolution of venomous animals and their toxins*. Toxinology. Springer. https://doi.org/10.1007/978-94-007-6458-3_19

Rayfield, E. J. (2007). Finite element analysis and understanding the biomechanics and evolution of living and fossil organisms. *Annual Review of Earth and Planetary Sciences*, *35*, 541–576.

Simone, L. R. L. (2011). Phylogeny of the Caenogastropoda (Mollusca), based on comparative morphology. *Arquivos de Zoologia*, *42*, 161–323.

Taylor, J. D. (1998). Understanding biodiversity: Adaptive radiations of predatory marine gastropods. In Morton, B. (Ed.), *The Marine Biology of the South China Sea. Proceedings of the Third International Conference on the Marine Biology of the South China Sea* (pp. 187–206). Hong Kong University Press.

Tyler, C. L., & Schiffbauer, J. D. (2012). The fidelity of microstructural drilling predation traces to gastropod radula morphology: Paleoecological applications. *Palaios*, *27*, 658–666.

Van der Wal, P., Giesen, H. J., & Videler, J. J. (1999). Radular teeth as models for the improvement of industrial cutting devices. *Materials Science and Engineering: C*, *7*, 129–142.

Vermeij, G. J. (1977). The Mesozoic marine revolution: Evidence from snails, predators and grazers. *Paleobiology*, *3*, 245–258.

Vermeij, G. J. (2001). Innovation and evolution at the edge: Origins and fates of gastropods with a labral tooth. *Biological Journal of the Linnean Society*, *72*, 461–508.

Vermeij, G. J., & Carlson, S. J. (2000). The muricid gastropod subfamily Rapaninae: Phylogeny and ecological history. *Paleobiology*, *26*, 19–46.

Wang, C., Li, Q. Y., Wang, S. N., Qu, S. X., & Wang, X. X. (2014). Microstructure and self-sharpening of the magnetite cap in chiton tooth. *Materials Science and Engineering: C*, *37*, 1–8.

Wealthall, R. J., Brooker, L. R., Macey, D. J., & Griffin, B. J. (2005). Fine structure of the mineralized teeth of the chiton *Acanthopleura echinata* (Mollusca: Polyplacophora). *Journal of Morphology*, *265*, 165–175.

Weaver, J. C., Wang, Q., Miserez, A., Tantuccio, A., Stromberg, R., Bozhilov, K. N., Maxwell, P., Nay, R., Heier, S. T., DiMasi, E., Kisailus, D. (2010). Analysis of an ultra hard magnetic biomineral in chiton radular teeth. *Materials Today*, *13*, 42–52.

SUPPORTING INFORMATION

Additional supporting information can be found online in the Supporting Information section at the end of this article.

How to cite this article: Herbert, G. S., Hill, S. A., Pio, M. J., Carney, R., Carlson, A., Newham, E., & Bright, J. A. (2023). Three-dimensional visualization of predatory gastropod feeding teeth with synchrotron scanning. *Journal of Morphology*, *284*, e21633. https://doi.org/10.1002/jmor.21633